Chapter 6

Results

This chapter presents two main results obtained regarding the model. First a validation through a synthetic example is developed. Then using a pair of angiographic image sequences the model is built and measurements are made on different vessel parameters like velocity, shape change, etc.

6.1 Experimental Results

Results of the vessel detection process using the contrast coherence learning.

To illustrate the viability of the *eigensnakes*, a real application of detecting coronary vessels in angiographies is considered. The approach is tested on 23 images and 5 different vessels. Using five scales for the filters with parameter $\rho = 9 \ldots 13$ and the following derivatives (up to third degree)

$$(\frac{d}{dx}, \frac{d}{dy}), (\frac{d^2}{dx^2}, \frac{d^2}{dy^2}), (\frac{d^2}{dxdy}, \frac{d^2}{dydx}), (\frac{d^3}{dx^3}, \frac{d^3}{dy^3}) \ \ and \ \ (\frac{d^3}{dxdxdy}, \frac{d^3}{dydxdx})$$

together with 5.12 we obtain 25 outputs per pixel. Adding the original image pixel the sampling dimension is 26. 130 points are learned, a data matrix $D_{m \times n}, m = 130, n = 26$ is constructed. Ought to the high number of pixels (samples) in any image, a dimensional space reduction by means of PCA is carried out from $n = 26$ to $l = 4$. In this experiment, the first four principal axes (eigenvectors) explain up to 99% of the variances according to

$$(e_i)\% = 100 * \lambda_i / \sum_{i=0}^{n-1} \lambda_i; \tag{6.1}$$

being e_i the percentage explained and λ_i the eigenvalues of $\mathbf{D}$ (fig. 5.6(c)).

For illustrative purposes a mahalanobis distance map is built projecting all image features onto the reduced space and measuring the distance to the training vessel cluster. The Mahalanobis distance map shows the snake convergence to a vessel. Due

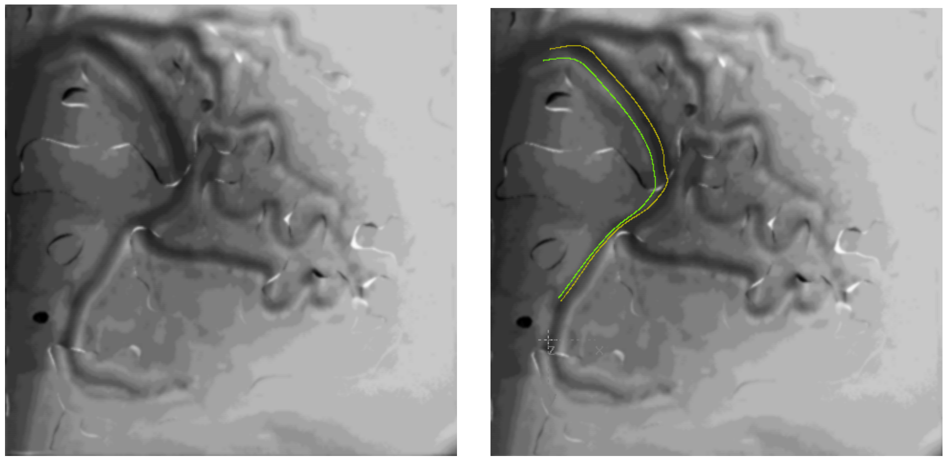

(a) (b)

Figure 6.1: Probabilistic external energy (a), Snake segmentation (b).

to the statistic learning, Mahalanobis distance is small mainly in vessel positions. As a result, false responses of vessel appearance are diminished and the snake local energy minima are significantly reduced. On the other hand, approaching the vessel, the Mahalanobis distance exponentially decreases driving the snake to lock on the vessel features. Figure 6.1(a) shows the probabilistic external energy map as a function of the Mahalanobis distance. In fig.6.1(b) a snake is used to segment a vessel. The snake has converged to the vessel in 30 iterations using the energy showed in figure 6.1(a). One can notice that in a real application the built-in map approach (5.14) is preferable to obtain faster energy-minimisation scheme avoiding explicit construction of likelihood map for the whole image.

6.1.1 Results of the vessel detection process using vessel profiles and PPCA.

Tha approach is tested in a vessel tracking framework. To demonstrate the viability of the tracking approach by statistic snakes, a hybrid potential maps is built to track a coronary tree vessel in a sequence of angiographies. The vessels are dynamic elastic elongated objects in images with very low contrast and signal-to-noise rate. A more sophisticated approach to segment and track objects is obligatory in order to achieve good results. For each image frame I in the sequence, a likelihood map is built and the minimized snake in frame $I-1$ is used as initialization. The first snake initialization is obtained using a path search through the vessel under analysis. The user provides the starting point of the path and the path search is carried out as follows: from the starting point the maximum likelihood vector is chosen and a set of coherence vectors is searched in the neighborhood for maximum scalar product. The process is repeated up to the end of the path (fig. 5.7(a)).

To build the maps a previous learning step is made with a set of twenty image frames. We take two hundred samples from each image and each sample is of forty pixels width. The sampled profiles are obtained perpendicular to the centerline of the vessels. To obtain the centerline, we use a conventional snake and the perpendicular profiles are defined regarding the snake. For each learned vessel we obtain a matrix where the rows are the profiles along a vessel (fig. 5.2). Within the probabilistic framework we make the dimensional reduction through PPCA using the first five principal axes, which explain up to 97% of the observed data variance in feature space.

The built map comprises the extraction of coherent directions through the second moment matrix (fig. 5.3) discarding regions with low module of the coherent vectors to speed up the process of map generation. Afterwards, the profiles over the extracted directions are obtained using as the middle point of the profile the origin of each direction vector. The profiles length, as in the learning step, is forty pixels. The profiles are then compared against the learned ones and as a result a measure of the probability of being a true vessel profile is obtained. Although this probability map can be considered ready to use (fig. 5.8), it is open to further refinements. Using more specific knowledge about the domain, we could recover the coherence directions and after weighting them with the probabilities we could test for parallelisms. Non parallel vectors mean high probability of being a false profile.

6.2 Model Validation

Using a phantom of a right coronary artery a set of images were acquired from a cardiac angiographic equipment. The acquisition was done providing a rotation movement of 47 degrees to the "C" arm at 12.5 frames per sec.. From a total of 64 frames acquired, the first 32 swapped from 0 degree Left Anterior Oblique (LAO) to 23.5 and the others from 23.5 LAO to 47 LAO. Note that the rotation axis of the "C" arm is labeled as X. The experiment consists of a $3D$ reconstruction using pair of frames from both groups. The expected result is a rotation of the model.

The model of the RCA split in four segments (R1, R2, R3, and R4) with three points per segment sum a total of 12 points. The points are named using the words proximal, middle and distal, indicating the position of each point withing the segment and regarding the ostium as the origin. Also, the segment number increases with the distance to the ostium. From the 32 frames of each group, we took 1 every 4 for a total of 8 samples (the acquisition speed is 3.125 frames per sec.).

The expected result was measured testing the following:

- Invariance of the distance to the origin of coordinates
- Invariance of the minimal distance to the rotation axis
- Speed: points near the rotation axis have lower speed than points far from it.
- Path length: points near the rotation axis describe a distance shorter than points far from it.

For each point in every sampled frame, the distance to the origin, and to the rotation axis was computed. Also speed and space between points in consecutive frames were computed. Finally, mean values and mean deviation was computed:

Mean:

$$\bar{x} = \frac{\sum_{i=1}^{n}(x_i)}{n}$$

Mean deviation:

$$\sigma = \frac{\sum_{i=1}^{n}|x_i - \bar{x}|}{n}$$

Tables 6.1 to 6.11 summarize the values obtained in the experiment.
Table 6.1 shows the distances to the rotation axis of the three points representing each segment. Table 6.2 shows the mean distances to the rotation axis of the three points representing each segment, and table 6.3 is the mean deviation.
Tables 6.4, 6.5 and 6.6 are the point speed measured as the space between two consequtive frames, the mean speed for each point and the mean deviation respectively.
Table 6.7 shows the lenght of the trajectory of the points between consecutive frames.
Table 6.8 shows the distances covered by the points during the 8 frames, and table 6.9 is the distance mean deviation. Finally, tables 6.10 and 6.11 depict the distamnces of the points to the origin of coordinated and their mean deviation respectively.

	1 $R1_{prox}$	2 $R1_{mid}$	3 $R1_{dist}$	4 $R2_{prox}$	5 $R2_{mid}$	6 $R2_{dist}$
0	40,934	26,124	27,812	34,289	32,821	31,254
1	41,635	26,620	26,553	32,777	32,021	30,368
2	44,519	27,452	25,310	31,311	31,060	30,599
3	46,585	28,478	25,770	31,402	30,373	30,123
4	45,462	26,549	24,995	30,769	30,932	30,583
5	42,524	27,115	25,138	30,611	30,641	30,753
6	45,537	30,370	25,728	29,477	30,496	31,480
7	38,862	29,822	26,603	29,447	30,583	31,720

	7 $R3_{prox}$	8 $R3_{mid}$	9 $R3_{dist}$	10 $R4_{prox}$	11 $R4_{mid}$	12 $R4_{dist}$
0	38,189	46,452	47,372	35,419	19,399	16,646
1	37,768	46,464	47,196	36,784	18,522	18,596
2	36,118	44,568	45,923	33,488	18,073	18,563
3	35,194	44,118	43,902	34,520	18,478	18,587
4	36,132	43,260	42,549	32,759	18,284	17,155
5	36,379	41,102	42,117	30,877	17,894	17,487
6	36,982	39,844	42,036	32,879	19,291	16,446
7	35,909	40,493	40,554	33,410	19,832	15,346

Table 6.1: Distance to the rotation axis (mm).

1 $R1_{prox}$	2 $R1_{mid}$	3 $R1_{dist}$	4 $R2_{prox}$	5 $R2_{mid}$	6 $R2_{dist}$
43,257	27,816	25,989	31,260	31,116	30,860
7 $R3_{prox}$	**8 $R3_{mid}$**	**9 $R3_{dist}$**	**10 $R4_{prox}$**	**11 $R4_{mid}$**	**12 $R4_{dist}$**
36,584	43,288	43,956	33,767	18,722	17,353

Table 6.2: Mean Distance to the rotation axis (mm).

1 $R1_{prox}$	2 $R1_{mid}$	3 $R1_{dist}$	4 $R2_{prox}$	5 $R2_{mid}$	6 $R2_{dist}$
2,269	1,305	0,750	1,184	0,653	0,469
7 $R3_{prox}$	8 $R3_{mid}$	9 $R3_{dist}$	10 $R4_{prox}$	11 $R4_{mid}$	12 $R4_{dist}$
0,797	2,113	2,156	1,356	0,589	0,955

Table 6.3: Distance Mean Deviation (rotation axis).

	1 $R1_{prox}$	2 $R1_{mid}$	3 $R1_{dist}$	4 $R2_{prox}$	5 $R2_{mid}$	6 $R2_{dist}$
0 to 1	11,609	7,241	12,585	9,723	8,011	11,985
1 to 2	15,954	10,174	12,143	16,427	14,220	9,236
2 to 3	11,823	10,281	5,430	5,623	10,647	8,969
3 to 4	5,139	8,328	13,388	9,471	2,753	13,172
4 to 5	10,030	7,738	3,425	9,521	8,996	8,732
5 to 6	12,691	18,174	6,227	13,450	22,108	11,489
6 to 7	21,351	4,623	7,723	9,043	4,371	4,329

	7 $R3_{prox}$	8 $R3_{mid}$	9 $R3_{dist}$	10 $R4_{prox}$	11 $R4_{mid}$	12 $R4_{dist}$
0 to 1	11,763	6,769	17,644	7,508	6,112	8,671
1 to 2	13,763	16,605	9,578	18,700	13,841	3,022
2 to 3	18,158	10,303	20,508	6,567	2,803	3,235
3 to 4	8,462	14,630	12,400	6,968	5,935	4,603
4 to 5	11,923	21,446	26,497	12,323	6,615	5,361
5 to 6	13,262	13,589	7,850	12,009	6,214	3,593
6 to 7	9,230	15,740	19,798	15,786	7,755	3,746

Table 6.4: Velocity (mm/seg).

1 $R1_{prox}$	2 $R1_{mid}$	3 $R1_{dist}$	4 $R2_{prox}$	5 $R2_{mid}$	6 $R2_{dist}$
13,744	8,898	8,580	10,288	9,434	9,030
7 $R3_{prox}$	8 $R3_{mid}$	9 $R3_{dist}$	10 $R4_{prox}$	11 $R4_{mid}$	12 $R4_{dist}$
11,974	14,353	16,759	11,956	7,129	4,497

Table 6.5: Mean Velocity.

1 $R1_{prox}$	2 $R1_{mid}$	3 $R1_{dist}$	4 $R2_{prox}$	5 $R2_{mid}$	6 $R2_{dist}$
4,357	2,984	3,094	2,326	4,668	2,440
7 $R3_{prox}$	8 $R3_{mid}$	9 $R3_{dist}$	10 $R4_{prox}$	11 $R4_{mid}$	12 $R4_{dist}$
2,316	3,099	5,112	3,706	1,991	1,286

Table 6.6: Velocity Mean Deviation.

	1 $R1_{prox}$	2 $R1_{mid}$	3 $R1_{dist}$	4 $R2_{prox}$	5 $R2_{mid}$	6 $R2_{dist}$
0 to 1	3,715	2,317	4,027	3,111	2,564	3,835
1 to 2	5,105	3,256	3,886	5,257	4,550	2,955
2 to 3	3,783	3,290	1,738	1,799	3,407	2,870
3 to 4	1,644	2,665	4,284	3,031	0,881	4,215
4 to 5	3,210	2,476	1,096	3,047	2,879	2,794
5 to 6	4,061	5,816	1,993	4,304	7,074	3,677
6 to 7	6,832	1,479	2,471	2,894	1,399	1,385
	7 $R3_{prox}$	8 $R3_{mid}$	9 $R3_{dist}$	10 $R4_{prox}$	11 $R4_{mid}$	12 $R4_{dist}$
0 to 1	3,764	2,166	5,646	2,402	1,956	2,775
1 to 2	4,404	5,314	3,065	5,984	4,429	0,967
2 to 3	5,811	3,297	6,563	2,101	0,897	1,035
3 to 4	2,708	4,682	3,968	2,230	1,899	1,473
4 to 5	3,815	6,863	8,479	3,943	2,117	1,716
5 to 6	4,244	4,349	2,512	3,843	1,988	1,150
6 to 7	2,954	5,037	6,335	5,052	2,482	1,199

Table 6.7: Path length (mm).

1 $R1_{prox}$	2 $R1_{mid}$	3 $R1_{dist}$	4 $R2_{prox}$	5 $R2_{mid}$	6 $R2_{dist}$
28,351	21,299	19,495	23,442	22,753	21,732
7 $R3_{prox}$	8 $R3_{mid}$	9 $R3_{dist}$	10 $R4_{prox}$	11 $R4_{mid}$	12 $R4_{dist}$
27,700	31,706	36,568	25,555	15,768	10,314

Table 6.8: Total path length of each point (mm).

1 $R1_{prox}$	2 $R1_{mid}$	3 $R1_{dist}$	4 $R2_{prox}$	5 $R2_{mid}$	6 $R2_{dist}$
1,100	0,924	1,098	0,818	1,509	0,689
7 $R3_{prox}$	8 $R3_{mid}$	9 $R3_{dist}$	10 $R4_{prox}$	11 $R4_{mid}$	12 $R4_{dist}$
0,739	1,079	1,751	1,205	0,687	0,441

Table 6.9: Mean Deviation of the path length.

	1 $R1_{prox}$	2 $R1_{mid}$	3 $R1_{dist}$	4 $R2_{prox}$	5 $R2_{mid}$	6 $R2_{dist}$
0	45,539	29,789	33,023	37,191	33,084	33,183
1	46,168	30,205	32,005	35,685	32,240	32,334
2	49,200	30,914	30,928	34,397	31,359	32,590
3	50,786	31,798	31,174	34,317	30,650	32,001
4	49,787	30,126	30,509	33,880	31,230	32,475
5	46,907	30,437	30,913	33,780	30,940	32,680
6	50,049	33,457	31,405	32,738	30,795	33,408
7	43,549	32,974	32,053	32,521	30,871	33,627
	7 $R3_{prox}$	8 $R3_{mid}$	9 $R3_{dist}$	10 $R4_{prox}$	11 $R4_{mid}$	12 $R4_{dist}$
0	43,144	53,372	57,394	51,217	39,580	30,483
1	42,899	53,642	55,727	52,152	39,375	31,478
2	41,218	51,608	55,920	49,951	38,988	31,485
3	40,236	51,268	53,259	50,559	39,686	31,795
4	41,761	50,832	53,238	49,800	39,684	30,713
5	41,916	47,575	50,981	48,122	38,724	30,420
6	42,316	46,225	51,082	49,350	39,843	30,179
7	40,772	47,376	50,660	49,527	40,549	29,688

Table 6.10: Distance to the origin (mm).

1 $R1_{prox}$	2 $R1_{mid}$	3 $R1_{dist}$	4 $R2_{prox}$	5 $R2_{mid}$	6 $R2_{dist}$
2,207	1,148	0,644	1,084	0,633	0,464
7 $R3_{prox}$	8 $R3_{mid}$	9 $R3_{dist}$	10 $R4_{prox}$	11 $R4_{mid}$	12 $R4_{dist}$
0,786	2,384	2,111	0,919	0,393	0,604

Table 6.11: Mean Deviation of the distance to the origin.

Chart 6.2 confirms the hypothesis made about speed, distances traveled and mean distances. Figure 6.3 depicts a frame of the results. The spacial speed (shape deformation) is showed through a colour coding. The coding uses blue, green, red to represent increasing speed in this order (blue means lower speed, red higher). and on the left there are the trajectories of the phanthom projections.

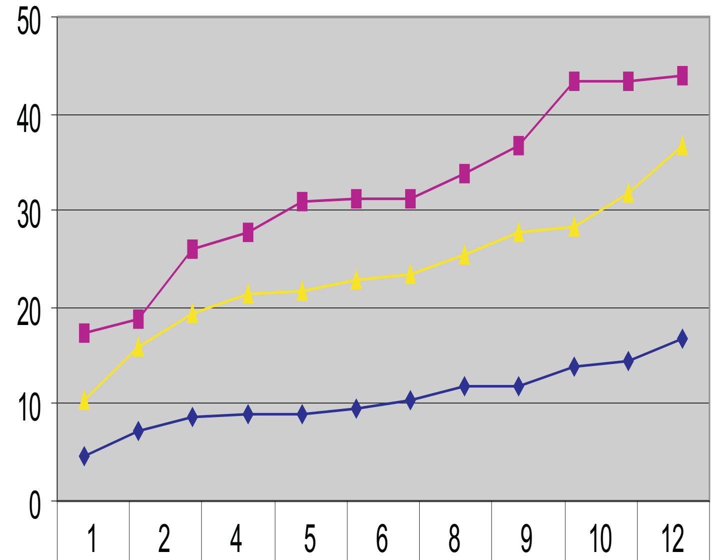

	1	2	4	5	6	8	9	10	12
Mean Velocity	4,497	7,129	8,898	9,03	9,434	11,956	11,974	13,744	16,759
Mean distance	17,353	18,722	27,816	30,86	31,116	33,767	36,584	43,257	43,956
Travelled distance	10,314	15,768	21,299	21,732	22,753	25,555	27,7	28,351	36,568

Figure 6.2: Point position, velocity (mm/seg) and traveled path (mm) regarding the rotation axis sorted by the distance to the axis. Points near the axis have less speed and shorter traveled path.

6.3 Results using real data

In this example the movement reconstruction and analysis with a real image sequence is presented.

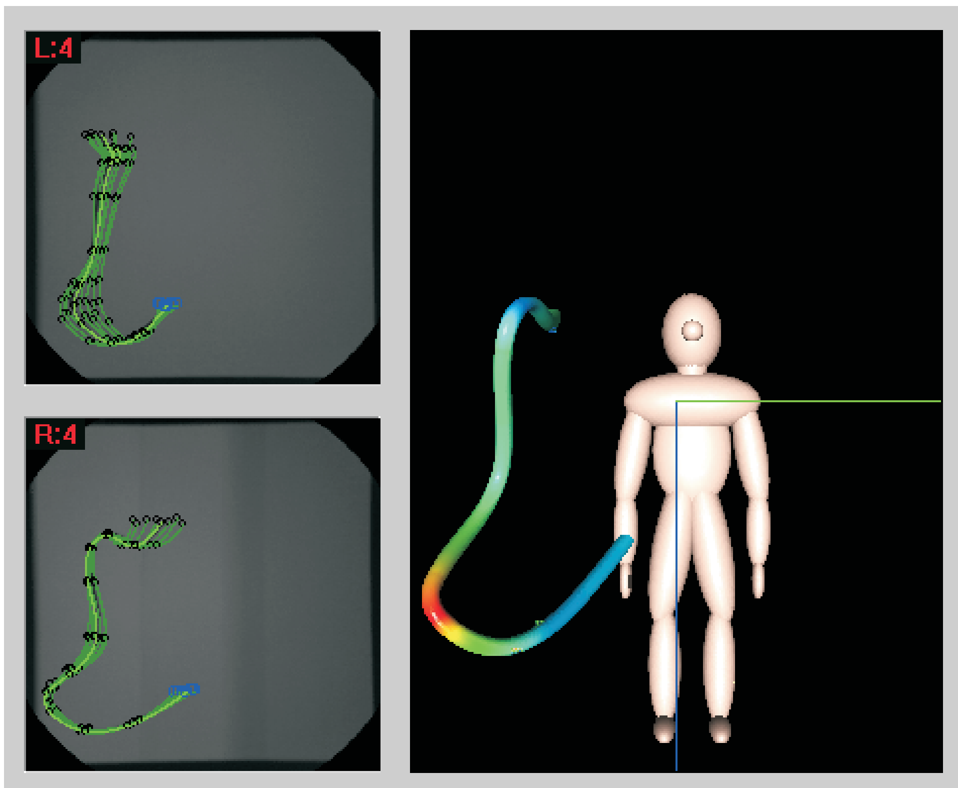

Figure 6.3: Fourth frame spatial speed using a colour coding and the phantom trajetory in both projections.

6.3.1 Case using (28.2 RAO, 0 Cranial) and (28.2 RAO, 19.8 Cranial) projection parameters.

These parameters allow for an optimal view of the left coronary arteries. Figure 6.4 shows the model and the selected arteries (red). The sequence under analysis consists

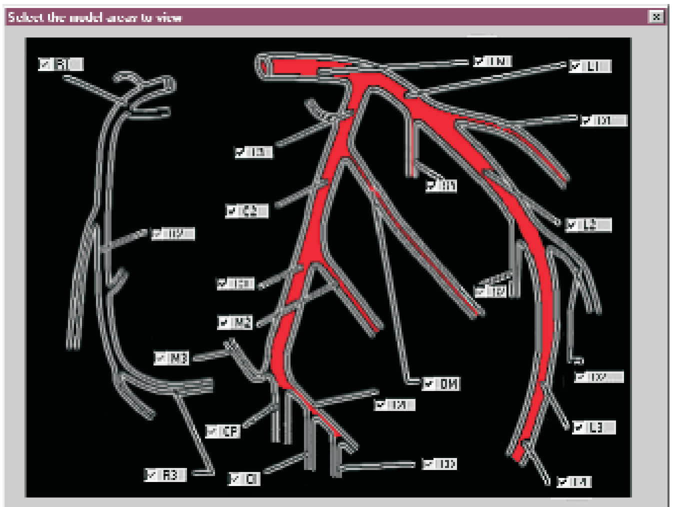

Figure 6.4: Selecting artery segments: LM, C1, C2, C3, C4, OM, M2, L1, L2, L3, L4, D1, D2, S1 i S2.

of six frames acquired at, aproximately 4 frames/sec. Then, the model was adapted to the angiographies. As the bifurcation are not detected the detection and tracking is done at branch level. Nevertheless the result is a superposition of every branch (Fig. 6.5).

Figure 6.6 shows the sequence after $3D$ reconstruction using B-splines.

Figure 6.7 shows the trajectories of the model branches in 2D and 3D.

Table 6.13 summarizes the space increment of every point between any two frames, total and mean traveled space for each frame. Segment C4 shows the highest increment (frame 1, 2).

Figure 6.8 shows the velocity at some points. The cyclic shape described by every point can be explained by the intrinsic beating of the heart, where the arteries are laying.

Table 6.14 shows that the point with highest mean speed is $C4_{prox}$ and the highest acceleration corresponds to frames 1 and 2. The values in the table are used to show the velocity as a mapping of colors.

Figure 6.9 shows the speed as a function of the time. In red, one can appreciate the highest change between frames 1 and 2. Meanwhile, the lowest change corresponds to frames 4 and 5 (blue). Transition between low and high is represented in green and yelow.

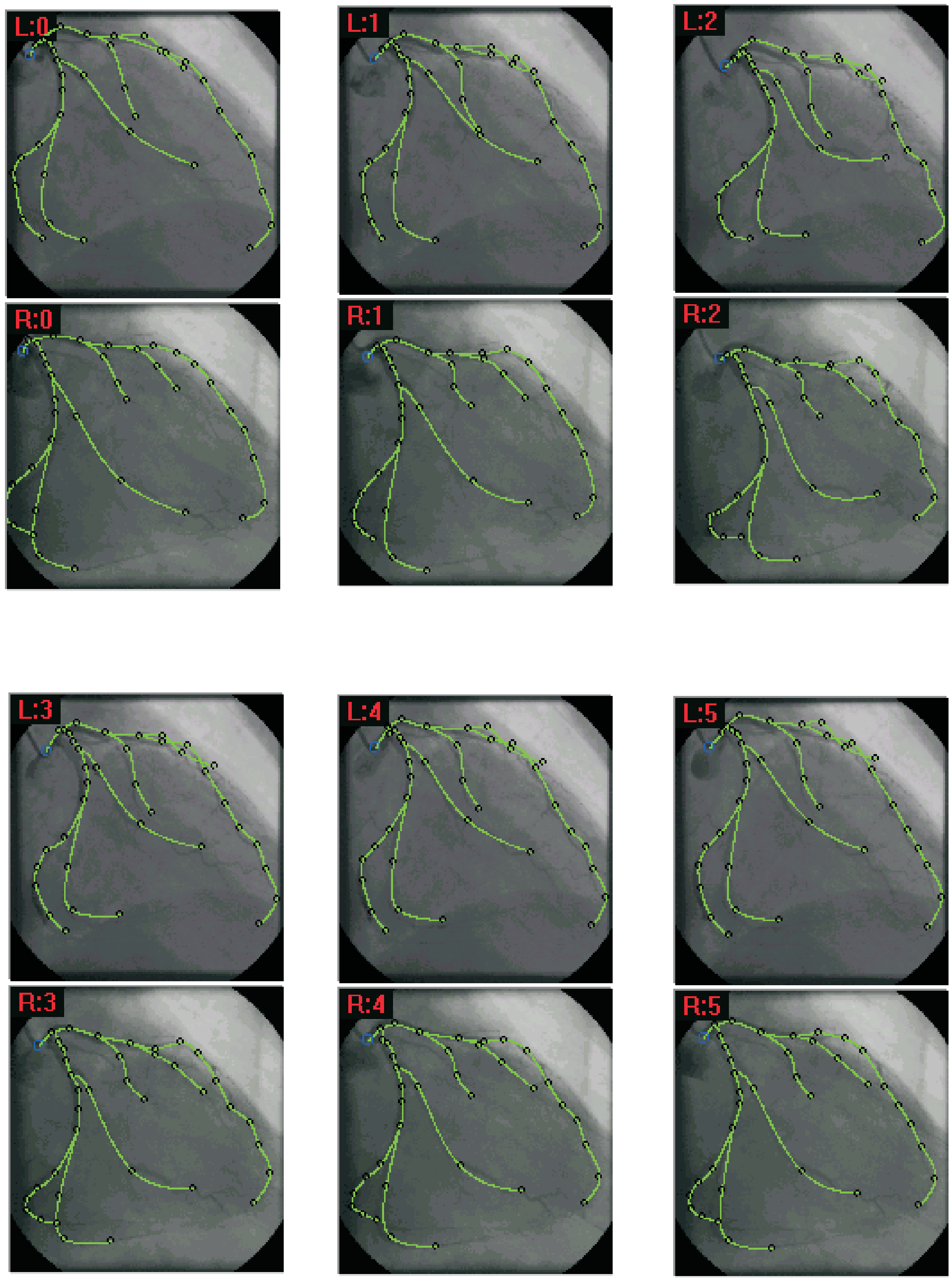

Figure 6.5: Model adapted.

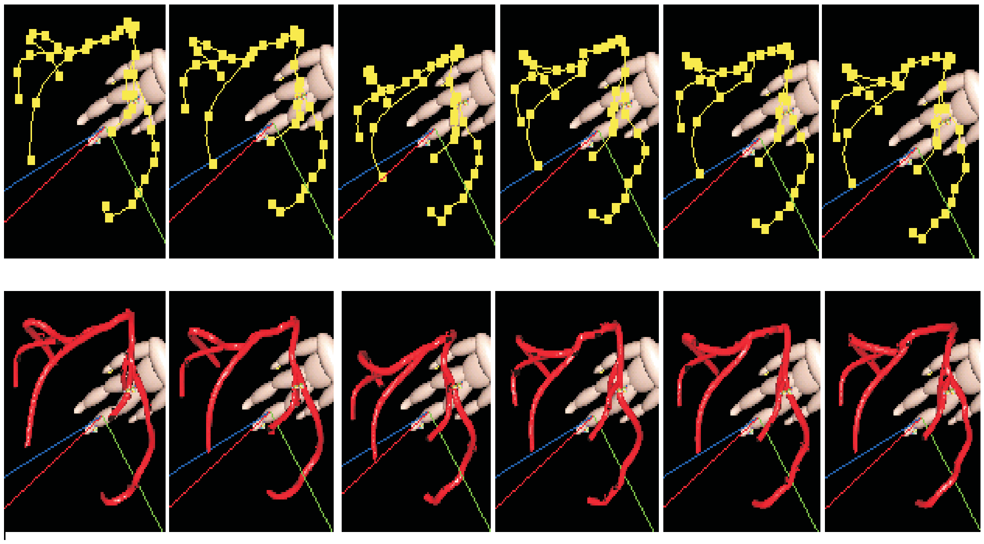

Figure 6.6: 3D Sequence Frames using bsplines and NURBS.

Figure 6.10 shows the dynamic behaviour of the shape of the arteries. The information is obtained, also, from table 6.14. The colour coding is also the same. At the first frames the higher speeds are near the ventricular zone, while during the last frames the high speed is showed near the auricular zone.

Using the right most column of table 6.14 and the same colour convention figure 6.11 shows the mean velocity. The circunflex artery shows the greatest global movement and the speed falls towards the apex.

Figure 6.12 shows a velocity threshold. One can split the speed in two categories setting a limit as a threshold. Using a colour coding the tree is displayed in two color matching speeds higher and lower than the threshold.

The following tables are the values used above.

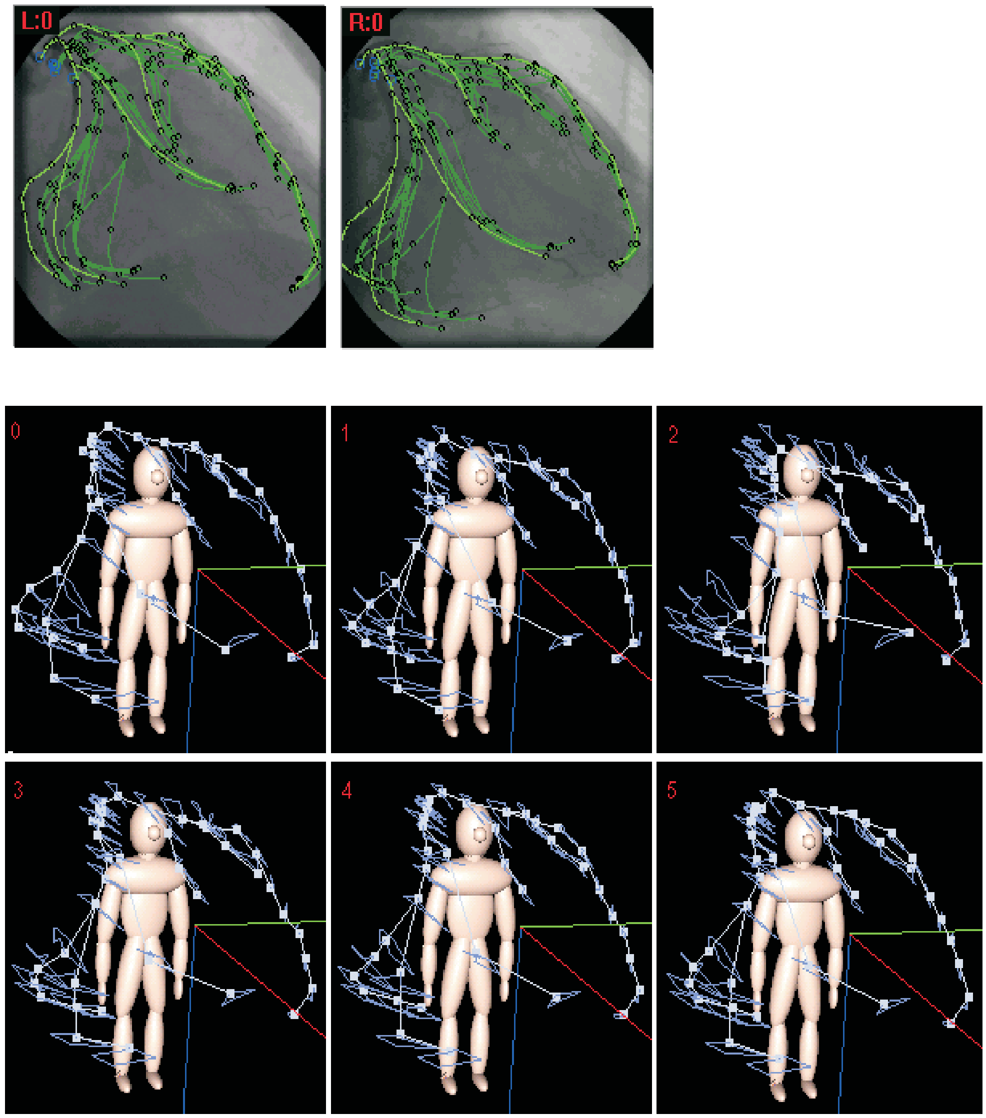

Figure 6.7: 2D and 3D Trajectories.

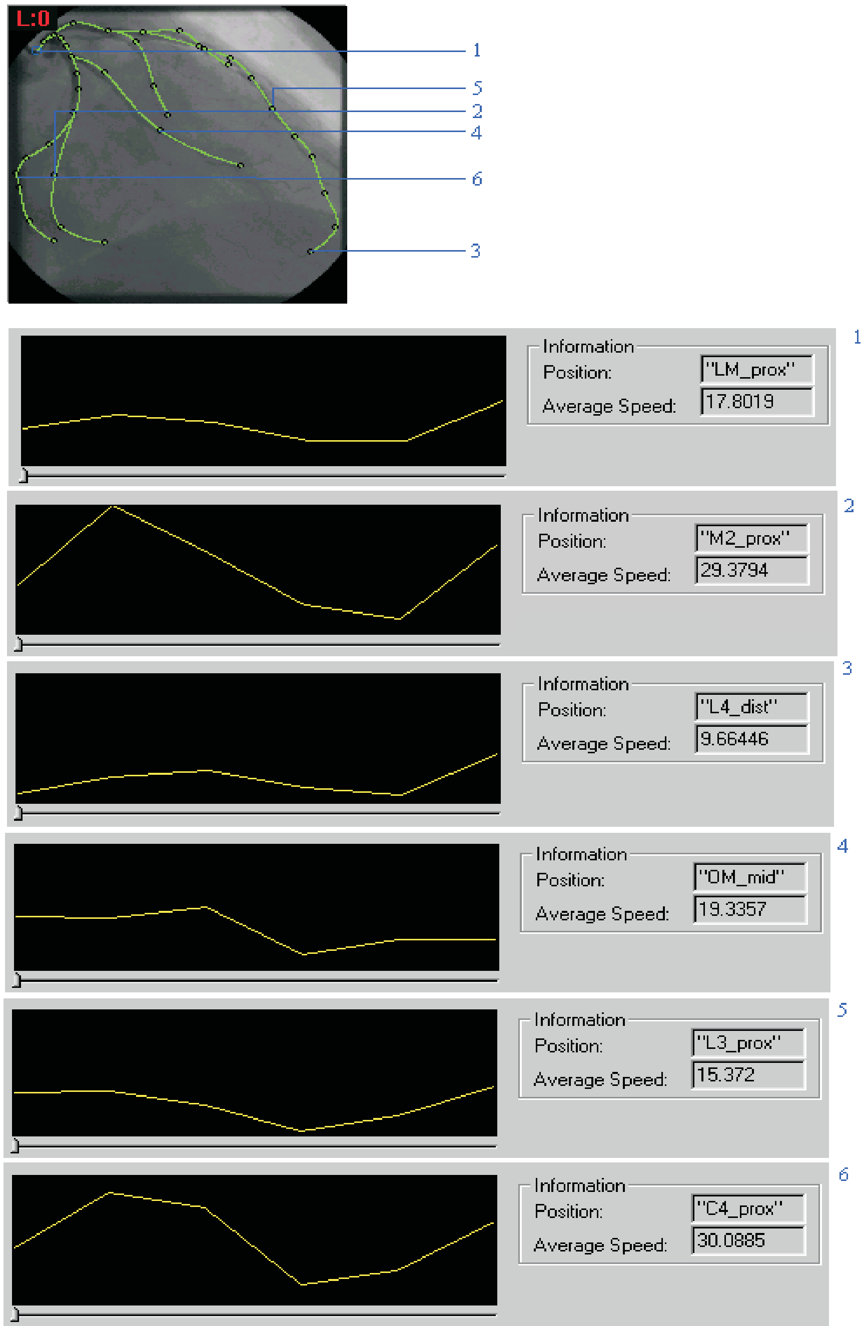

Figure 6.8: Velocity at different artery points.

		Frame 0	Frame 1	Frame 2	Frame 3	Frame 4	Frame 5
1	LM_{prox}	65,727	59,400	52,119	58,561	59,301	61,000
2	LM_{mid}	66,012	59,103	51,228	58,980	60,455	60,724
3	LM_{dist}	64,967	58,549	50,587	59,268	58,235	60,698
4	$C1_{prox}$	63,194	57,195	49,271	57,744	59,427	60,754
5	$C1_{mid}$	60,382	54,563	46,682	57,067	59,277	63,258
6	$C1_{dist}$	58,567	57,819	46,648	59,631	60,386	61,402
7	$C2_{prox}$	58,839	54,560	45,231	50,938	55,198	56,705
8	$C2_{mid}$	54,363	50,081	45,897	51,236	52,784	49,887
9	$C2_{dist}$	55,489	55,501	46,266	54,860	53,917	52,162
10	$C3_{prox}$	60,502	56,951	56,174	63,656	64,900	66,988
11	$C3_{mid}$	71,166	67,871	61,178	73,060	65,544	71,491
12	$C3_{dist}$	77,672	76,717	60,106	71,412	73,401	70,705
13	$C4_{prox}$	77,324	70,975	59,304	69,140	69,635	66,374
14	$C4_{mid}$	65,342	62,190	55,030	59,051	59,323	58,187
15	$C4_{dist}$	59,320	59,173	49,823	55,427	57,036	56,213
16	$M2_{prox}$	70,678	67,252	48,431	58,938	56,828	55,849
17	$M2_{mid}$	73,443	70,908	59,087	66,448	65,755	66,213
18	$M2_{dist}$	66,689	65,938	56,215	57,474	58,769	59,720
19	OM_{prox}	71,922	58,869	42,591	49,105	49,516	54,185
20	OM_{mid}	66,442	62,379	51,969	63,385	61,807	67,841
21	OM_{dist}	60,741	60,427	58,292	59,173	57,933	63,352
22	$L1_{prox}$	63,963	57,744	52,273	56,879	59,100	60,788
23	$L1_{mid}$	54,941	47,935	43,959	46,984	51,037	52,679
24	$L1_{dist}$	49,612	42,716	37,573	40,809	44,687	47,530
25	$L2_{prox}$	41,162	37,602	34,540	37,800	39,196	41,394
26	$L2_{mid}$	39,418	39,110	37,429	38,084	40,395	40,395
27	$L2_{dist}$	40,112	40,467	38,203	37,728	39,524	39,524
28	$L3_{prox}$	42,048	45,124	40,320	37,842	38,767	37,467
29	$L3_{mid}$	44,007	46,358	44,425	38,961	42,715	42,605
30	$L3_{dist}$	47,706	48,086	49,386	46,729	47,751	45,926
31	$L4_{prox}$	56,207	55,479	52,386	50,362	49,825	48,150
32	$L4_{mid}$	59,143	60,895	62,755	58,906	57,096	56,482
33	$L4_{dist}$	59,995	59,968	59,604	57,213	58,057	58,057
34	$D1_{prox}$	48,196	42,074	38,817	46,012	47,737	50,504
35	$D1_{mid}$	42,001	35,893	34,051	37,967	39,313	40,472
36	$D1_{dist}$	43,827	50,493	47,682	50,353	50,595	50,865
37	$S1_{prox}$	46,839	35,318	30,813	37,476	39,341	40,815
38	$S1_{mid}$	28,540	25,243	18,042	22,178	24,427	24,983
39	$S1_{dist}$	24,156	24,566	18,692	14,247	16,841	15,410

Table 6.12: Distances to the origin of coordinates (mm).

	Frame 0	Frame 1	Frame 2	Frame 3	Frame 4	Frame 5	Tot. Space
LM_{prox}	5,113	7,194	6,037	3,223	3,379	9,234	34,180
LM_{mid}	5,890	6,521	8,505	2,242	6,969	6,251	36,378
LM_{dist}	5,890	6,521	9,409	7,682	4,455	6,410	40,368
$C1_{prox}$	5,890	6,521	7,333	2,936	2,984	7,973	33,636
$C1_{mid}$	5,890	6,521	9,218	2,000	6,407	15,027	45,062
$C1_{dist}$	10,152	9,440	11,762	3,878	2,756	12,681	50,669
$C2_{prox}$	5,890	8,078	5,795	3,538	3,048	7,228	33,576
$C2_{mid}$	5,890	9,512	7,045	3,755	2,674	5,688	34,564
$C2_{dist}$	7,414	12,359	10,702	3,919	2,689	4,589	41,672
$C3_{prox}$	5,890	12,255	8,907	3,879	1,898	12,940	45,770
$C3_{mid}$	7,262	11,000	13,600	8,342	5,459	9,781	55,444
$C3_{dist}$	8,196	18,953	12,854	3,749	3,237	6,717	53,707
$C4_{prox}$	8,133	16,387	13,930	2,725	4,706	11,889	57,770
$C4_{mid}$	7,050	11,885	6,553	3,724	2,374	10,472	42,059
$C4_{dist}$	4,574	10,991	8,729	3,594	2,329	9,666	39,882
$M2_{prox}$	6,953	18,746	11,763	3,885	2,000	13,060	56,409
$M2_{mid}$	6,953	13,742	11,264	1,622	1,204	7,199	41,984
$M2_{dist}$	6,953	13,375	8,413	1,628	1,789	10,021	42,179
OM_{prox}	6,810	14,002	6,243	2,409	4,945	12,737	47,145
OM_{mid}	8,087	7,849	9,427	2,409	4,693	4,660	37,124
OM_{dist}	10,211	5,612	7,492	1,328	4,945	5,999	35,587
$L1_{prox}$	5,083	6,579	6,387	2,380	2,711	3,935	27,074
$L1_{mid}$	8,776	6,579	10,993	3,382	5,863	7,287	42,880
$L1_{dist}$	5,806	5,061	2,737	3,627	2,300	6,223	25,755
$L2_{prox}$	4,193	6,591	5,914	4,474	5,461	1,406	28,039
$L2_{mid}$	0,747	6,507	7,492	2,045	1,724	3,725	22,240
$L2_{dist}$	2,794	5,597	5,375	1,792	0,669	0,738	16,965
$L3_{prox}$	6,540	6,808	4,738	0,859	3,079	7,491	29,514
$L3_{mid}$	4,964	3,856	7,535	4,154	0,937	2,528	23,975
$L3_{dist}$	2,598	2,953	3,976	2,609	1,727	2,836	16,700
$L4_{prox}$	0,747	10,676	4,343	0,646	2,660	12,562	31,634
$L4_{mid}$	5,730	2,177	4,947	4,588	1,149	5,538	24,130
$L4_{dist}$	1,116	3,505	4,410	1,876	0,783	6,865	18,556
$D1_{prox}$	7,165	5,061	8,751	4,531	2,260	6,941	34,709
$D1_{mid}$	7,777	5,061	6,980	2,185	1,674	4,490	28,167
$D1_{dist}$	9,510	6,025	3,591	2,185	1,674	9,910	32,895
$S1_{prox}$	11,447	6,579	6,809	2,185	3,163	6,623	36,806
$S1_{mid}$	10,642	6,579	8,019	2,185	3,163	4,581	35,168
$S1_{dist}$	7,319	6,579	8,019	2,185	3,163	9,099	36,362
Mean	6,360	8,467	7,846	3,086	3,053	7,512	

Table 6.13: Increment, mean and total space (mm).

	Frame 0	Frame 1	Frame 2	Frame 3	Frame 4	Frame 5	Mean/Point
LM_{prox}	15,978	22,481	18,865	10,072	10,561	28,855	17,802
LM_{mid}	18,405	20,379	26,577	7,007	21,778	19,534	18,947
LM_{dist}	18,405	20,379	29,404	24,007	13,923	20,032	21,025
$C1_{prox}$	18,405	20,379	22,914	9,176	9,324	24,915	17,519
$C1_{mid}$	18,405	20,379	28,805	6,250	20,021	46,960	23,470
$C1_{dist}$	31,726	29,499	36,756	12,117	8,613	39,629	26,390
$C2_{prox}$	18,405	25,243	18,109	11,057	9,524	22,586	17,487
$C2_{mid}$	18,405	29,726	22,017	11,734	8,356	17,775	18,002
$C2_{dist}$	23,169	38,623	33,442	12,246	8,403	14,341	21,704
$C3_{prox}$	18,405	38,298	27,834	12,123	5,932	40,439	23,838
$C3_{mid}$	22,694	34,375	42,499	26,069	17,060	30,566	28,877
$C3_{dist}$	25,612	59,228	40,169	11,717	10,117	20,991	27,973
$C4_{prox}$	25,415	51,209	43,532	8,516	14,706	37,153	30,088
$C4_{mid}$	22,032	37,140	20,477	11,638	7,420	32,726	21,906
$C4_{dist}$	14,293	34,345	27,277	11,232	7,278	30,205	20,772
$M2_{prox}$	21,729	58,582	36,760	12,142	6,251	40,813	29,379
$M2_{mid}$	21,729	42,944	35,200	5,070	3,762	22,495	21,867
$M2_{dist}$	21,729	41,796	26,291	5,086	5,592	31,315	21,968
OM_{prox}	21,280	43,756	19,511	7,527	15,453	39,802	24,555
OM_{mid}	25,273	24,527	29,459	7,527	14,665	14,563	19,336
OM_{dist}	31,909	17,538	23,412	4,149	15,453	18,747	18,535
$L1_{prox}$	15,884	20,558	19,961	7,436	8,470	12,296	14,101
$L1_{mid}$	27,424	20,558	34,354	10,570	18,321	22,772	22,333
$L1_{dist}$	18,143	15,816	8,554	11,334	7,188	19,448	13,414
$L2_{prox}$	13,103	20,596	18,483	13,982	17,065	4,393	14,604
$L2_{mid}$	2,336	20,334	23,412	6,392	5,386	11,640	11,583
$L2_{dist}$	8,732	17,491	16,797	5,601	2,089	2,305	8,836
$L3_{prox}$	20,437	21,275	14,806	2,683	9,621	23,409	15,372
$L3_{mid}$	15,513	12,051	23,546	12,982	2,930	7,901	12,487
$L3_{dist}$	8,120	9,227	12,426	8,154	5,397	8,863	8,698
$L4_{prox}$	2,336	33,363	13,571	2,019	8,312	39,255	16,476
$L4_{mid}$	17,907	6,802	15,460	14,338	3,591	17,307	12,568
$L4_{dist}$	3,489	10,954	13,782	5,861	2,448	21,452	9,664
$D1_{prox}$	22,390	15,816	27,347	14,159	7,064	21,691	18,078
$D1_{mid}$	24,303	15,816	21,814	6,827	5,233	14,031	14,670
$D1_{dist}$	29,718	18,827	11,223	6,827	5,233	30,969	17,133
$S1_{prox}$	35,773	20,558	21,279	6,827	9,884	20,698	19,170
$S1_{mid}$	33,255	20,558	25,058	6,827	9,884	14,316	18,316
$S1_{dist}$	22,872	20,558	25,058	6,827	9,884	28,433	18,939
Mean/Frame	19,875	26,461	24,519	9,644	9,543	23,478	

Table 6.14: Velocity and mean for each point and frame (mm/seg).

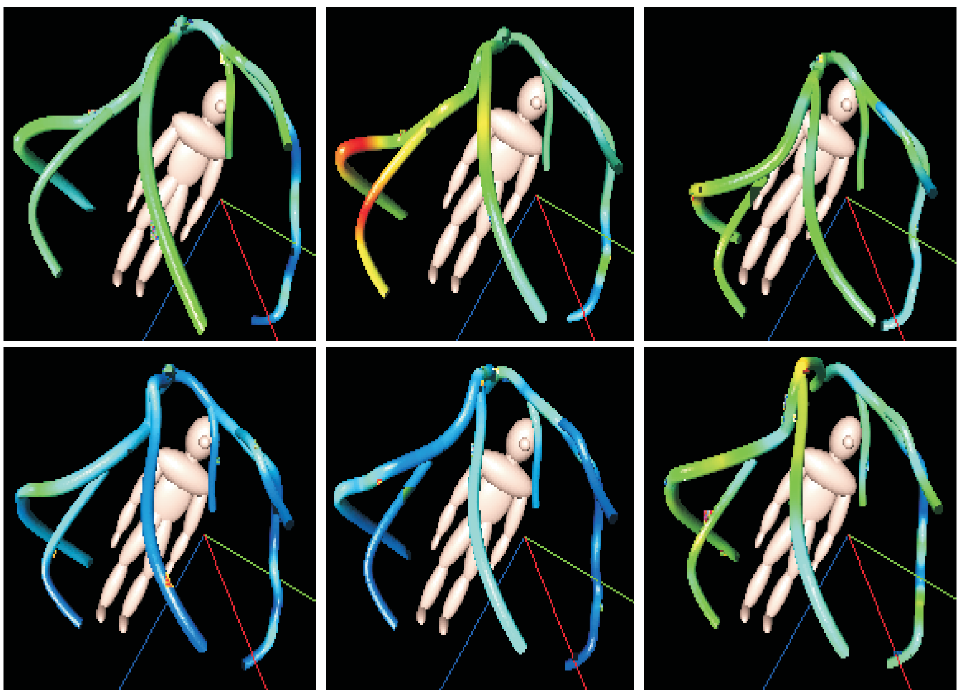

Figure 6.9: Temporal dynamic analysis.

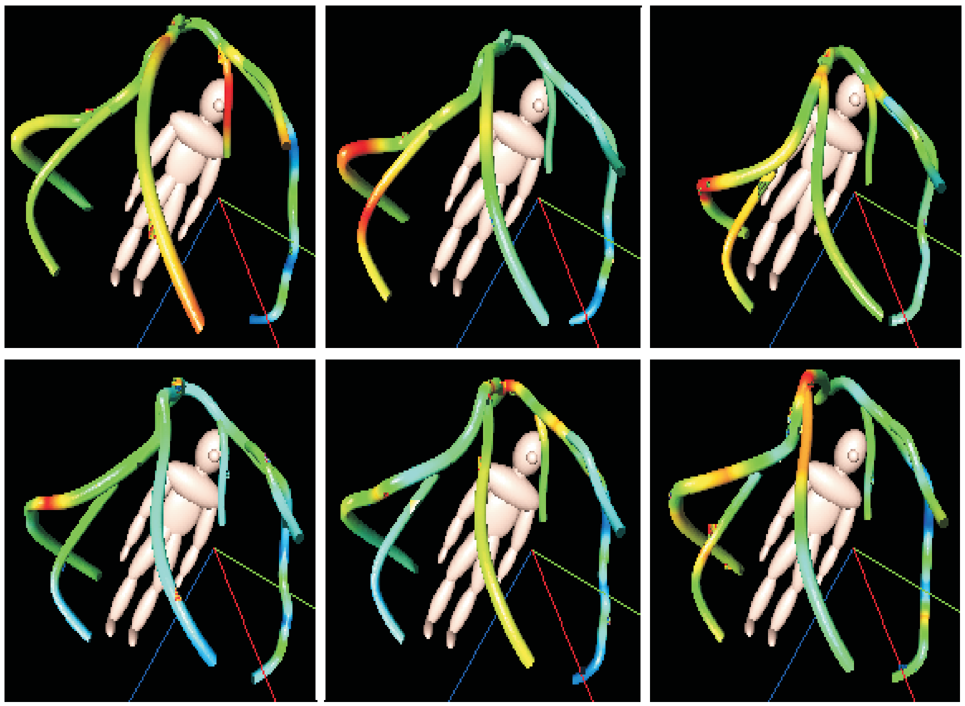

Figure 6.10: Shape dynamics analysis.

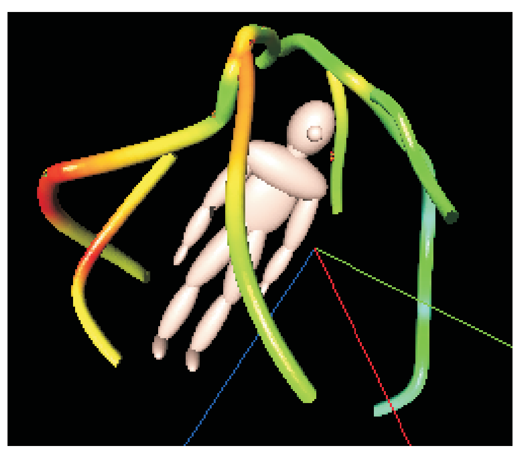

Figure 6.11: Mean speed.

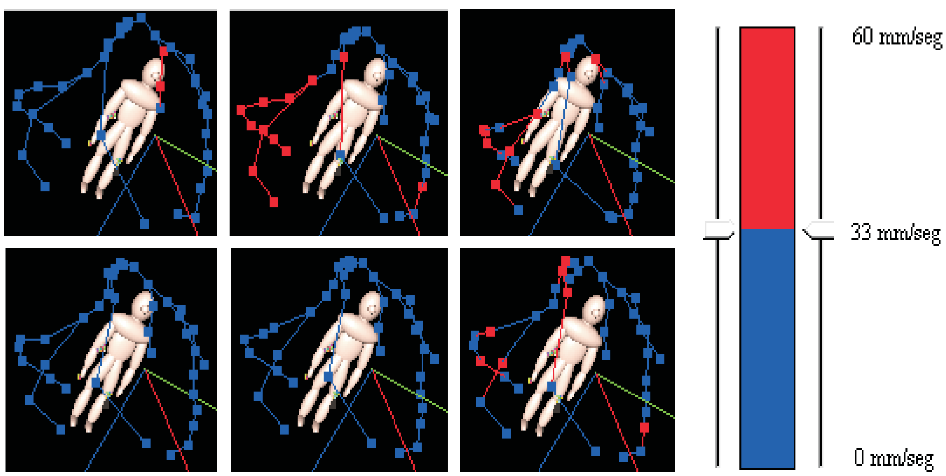

Figure 6.12: Setting a threshold to visualize areas of different speeds. In blue areas with speeds lower than 33 mm/seg otherwise in red.

The results obtained can be interpreted as follows: the heart beats in a cyclic way. To each dilation follows a contraction. In the case study, the first three frames correspond to the contraction period (systole) and the last ones to dilation (diastole). There is a qualitative coincidence (visual) between the $3D$ trajectories obtained and the systole/diastole cycle. The movement, in general, is greater during diastole.

Moreover, a quantitative analysis done using the data in the tables shows the same coincidence. For example, sorting the artery segments by mean velocity, greater to less: C3, M2, C4, C1, OM, LM, C2, S1, D1, L1, L4, L3, L2. However, it has to be clear that further clinical assessment and validation is necessary to use the model in a clinical daily work.

6.4 Summary

The chapter presents some experimental results obtained with the model. The data obtained agree with the expected data taking into account the qualitative dynamic behaviour of a heart (normal).

Chapter 7

Conclusion and future work

7.0.1 Main contributions

A deformable coronary tree model

Using snakes as a global technique and a graph structure to hold the information, a $3D$ model of the coronary arteries is developed. The model takes into account the intrinsic vessel deformation and the vessel movements. It is ready to incorporate more knowledge, like vessel diameter, acceleration, etc..

In order to build the model, there are two approaches to data collection: do it manually or automatically. In this thesis the data collection is done automatically. The global technique used is known as snakes and at this point are three main contributions: two of them are resumed in incorporating elements of probability and statistics and the third is related to $3D$ reconstruction.

Statistical snakes

A new minimizing schema for snakes is developed. At this point a statistical vessel learning is used together with a mahalanobis distance measure to obtain a new minimizing schema for the snake named by us as eigensnakes. The other contribution has consisted in replacing the deterministic potential map by a probabilistic one after a learning process of vessel gray profiles.

The value of the statistic basis for linear structure detection and tracking has been established by demonstrating two methods:

1. the mechanism of PCA and Mahalanobis distances embeded into the minimization eschema of the snakes.

2. the mechanism of the PPCA embedded into the snake framework.

In order to manage complex objects and the variability of appearance of image structures, our techniques are supported by a learning approach to extract and detect only these "crease-like" features determined by the training set. Learned models are used in a probabilistic framework in order to build significant energy potential, resulting in less false responses of the image feature detector and more robust snake-based object tracking.

A new approach to potential computation using a likelihood map is formulated and applied to the tracking of specific structure on angiographies. The snake is less dependent on its initialisation and once placed on the hybrid potential map it converges to image features with high probability to represent learned object profiles. The obtained results and the self-training capability of the snake encourage utilizing it in different applications.

The experiments carried out showed that there are no significative differences between the use of PCA or PPCA regarding the results (vessel detection). The PCA are faster to compute, meanwhile PPCA offers a probabilistic framework open to incorporate higher levels of reasoning.

3D Vessel reconstruction using snakes

Finally, a new approach for $3D$ reconstruction under uncertainty conditions using snakes is formulated. The aim is to take profit of the "global property" of the snakes at a curve level instead of using the usual point to point reconstruction strategy. A snake model was applied to segment and reconstruct the coronary vessels. The advantages of this approach are that no exact user-provided point correspondence is necessary. The snake evolves in the space to adjust to the image data; as a result the model provides such a correspondence between the image points. The results showed that the technique is optimal from the point of view of the minimal reconstruction error defined as the distance between the projection rays. Furthermore, the reconstruction is improved when isocenter co-ordinates are iteratively updated.

7.0.2 Results

A cardiac imaging workstation was developed. From an existing radiological imaging workstation, the evolution process was explained. The goal was on the conformance to the international standard formulated for digital imaging in medicine. A deformable coronary tree model. A model to enable a high degree of automation in computer vessel analysis from angiographic imaging.

7.0.3 Future work

Clinical research about coronary arteries dynamics. Full integration of the model into the cardiac image analysis software. Complete the model with statistically relevant data. Here an increment of samples are needed. Research to define new attributes to include in the graph. Image registration. To fuse spatial information from biplane angiograms with structural information provided by intra-vascular ultrasound images.

Bibliography

[1] ACR-NEMA. *ACR-NEMA Standards Publication/ N 300-1985.* ACR-NEMA, 1985.

[2] ACR-NEMA. *ACR-NEMA Standards Publication/ N 300-1988.* ACR-NEMA, 1988.

[3] Siemens AG and Philips Medical Systems. Spi - standard product interconnect for compatibility of digital imaging. Technical report, Siemens AG and Philips Medical Systems, 1987.

[4] E. Bardinet, L. D. Cohen, and N. Ayache. Superquadrics and free-form deformations: a global model to fit and track 3d medical data. *Proceedings of the First International Conference on Computer Vision, Virtual Reality and Robotics in Medicine*, pages 266–274, 1996.

[5] E. Bardinet, L. D. Cohen, and N. Ayache. Tracking medical 3d data with a deformable parametric model. *Proceedings of European Conference on Computer Vision*, 1:317–328, 1996.

[6] R. Bartels, J. Beatty, and B. Barsky. *An Introduction to Splines for use in Computer Graphics and Geometric Modeling*. Morgan Kaufmann Publishers. Inc, 1987.

[7] K. Barth, B. Eicker, and J. Seissl. Automated biplane vessel recognition in digital coronary angiograms. *Proceedings SPIE. Medical Imaging IV. Image Processing*, 1233:266–274, 1990.

[8] D.J. Bartholomew. *Latent Variable Models and Factor Analysis*. Charles Griffin and Co. Ltd., 1987.

[9] B. Bascle, P. Bouthemy, R. Deriche, and F. Meyer. Tracking complex primitives in an image sequence. *Proc. 12th IAPR International Conference on Pattern Recognition*, pages 426–431, 1994.

[10] M. Büchi, O. M. Hess, and R. L. Kirkeeide et al. Validation of a new automatic system for biplane quantitative coronary arteriography. *International Journal of Cardiac Imaging*, vol. 5:93–103, 1990.

[11] M. O. Berger. Snake growing. *Proceedings of European Conference on Computer Vision. Springer-Verlag*, pages 570–572, 1990.

[12] M. O. Berger. Tracking moving contours using energy-minimizing elastic contour models. *Proceedings of European Conference on Computer Vision. Springer-Verlag*, pages 453–457, 1992.

[13] W. D. Bidgood and S.C. Horii. *PACS Mini Refresher Course: Introduction to the ACR-NEMA DICOM Standard.* Radiographics, 1992.

[14] Christopher M. Bishop and Michael E. Tipping. Probabilistic principal component analysis. *Tech. Report NCGR*, 1997.

[15] Christopher M. Bishop and Michael E. Tipping. Mixtures of probabilistic principal component analysers. *Technical Report NCGR*, 1998.

[16] A. Blake, R. Curwen, and A. Zisserman. A framework for spatiotemporal control in the tracking of visual contours. *International journal of Computer Vision*, pages 127–145, 1993.

[17] A. Blake and M. Isard, editors. *Active ontours.* Springer Verlag, 1998.

[18] S. Y. J. Chen and J. D. Carroll. Dynamic reconstruction of 3d coronary arterial trees based on a sequence of biplane angiograms. *Proceedings of SPIE. Image Processing*, 3034:358–368, 1997.

[19] P. Coad and E. Yourdon. *Object-oriented Analysis, second edition.* Englewood Cliffs, NJ: Prentice-Hall, Inc., 1991.

[20] J. L. Coatrieux, R. Collorex, and C. Roux. Approaches for the three-dimensional reconstruction of coronary arteries: Review and prospects. *Critical Reviews in Bio. Eng.*, vol. 22 no. 1:1–38, 1994.

[21] J. L. Coatrieux, J. L. Rong, and R. Collorex. A framework for automatic analysis of the dynamic behaviour of coronary angiograms. *The International Journal of Cardiac Imaging*, 8:1–10, 1992.

[22] B. Coedhart and J.H.C. Reiber. *The Role of DICOM in the Digital Catheterisation Laboratory, in Cardiovascular Imaging, Eds. J.H.C. Reiber and E.E. van der Wall.* Dordrecht: Kluwer Academic Publishers, 1996.

[23] L. D. Cohen. On active contour models and balloons. *CVGIP: Image Understanding*, vol. 53 no. 2:211–2189, 1991.

[24] L. D. Cohen and I. Cohen. Deformable models for 3d medical images using finite elements & ballons. *International Conference on Computer Vision and Pattern Recognition*, pages 592–598, 1992.

[25] L. D. Cohen and I. Cohen. Finite-element methods for active contour models and balloons for 2-d and 3-d images. *IEEE Transactions on Pattern Analysis and Machine Intelligence*, 15(11):1131–1147, November 1993.

[26] ACR NEMA Committee. *Digital Imaging and Communications in Medicine (DICOM), parts 1-9. Standards Publication PS3.x.* National Electrical Manufacturers' Association, 1993.

[27] P.B. Condit, G. Pelanek, and T. Rourke. *Requirements for Cardiac Interchange Media and the Adoption of Recordable CD, in Cardiovascular Imaging, Eds. J.H.C. Reiber and E.E. van der Wall.* Dordrecht: Kluwer Academic Publishers, 1996.

[28] J.T. Cusma and T.M. Bashore. *The Digital Catheterization Laboratory - Is it Practical Today?, in Cardiovascular Imaging, Eds. J.H.C. Reiber and E.E. van der Wall.* Dordrecht: Kluwer Academic Publishers, 1996.

[29] C.A. Davatzikos and J. L. Prince. An active contour model for mapping the cortex. *IEEE Transactions on Medical Imaging*, 14(1):65–80, 1995.

[30] A.P. Dempster, N.P. Lair, and D.B. Rubin. Maximum likelihood from incomplete data via the EM algorithm. *Journal of the Royal Statistical Society Series B*, 39:1–38, 1977.

[31] T.S. Denney and J. L. Prince. Reconstruction of 3-d left ventricular motion from planar tagged images: an estimation theoretic approach. *IEEE Transactions on Medical Imaging*, 14(4):625–635, 1995.

[32] J. Dodge, G. Brown, and E. Bolson H. Dodge. Intrathoracic spatial location of specified coronary segments on the normal human heart. applications in quantitative arteriography, assessment of regional risk and contraction, and anatomic display. *Circulation*, 78:1167–1180, 1988.

[33] J. Dodge, G. Brown, and E. Bolson H. Dodge. Intrathoracic spatial location of specified coronary segments on the normal human heart. applications in quantitative arteriography, assessment of regional risk and contraction, and anatomic display. *Circulation*, 86:1167–1180, 1992.

[34] A. C. M. Dumay. *Image Reconstruction from Biplane Angiographic Projections.* PhD thesis, Technische Universiteit Delft. Netherlands, 1992.

[35] A.C.M. Dumay, J.H.C. Reiber, and J. J. Gerbrands. Determination of optimal angiographic viewing angles: Basic principles and evaluation study. *IEEE Transactions on Medical Imaging*, vol. 13 no. 1:13–23, 1994.

[36] G. J. Edwards, C. J. Taylor, and T. F. Cootes. Learning to identify and track faces in image sequences. *British Machine Vision Conference*, 8:130–139, 1997.

[37] J.H.C. Reiber et al. *State-of-the-art in Quantitative Coronary Arteriography as of 1996.* in Cardiovascular Imaging, Eds. J.H.C. Reiber and E.E. van der Wall. Dordrecht: Kluwer Academic Publishers, 1996.

[38] N. Fernandez, R. Toledo, and J. Villanueva. Visualización del Árbol coronario. Memoria de Proyecto de fin de Carrera. Universidad Autónoma de Barcelona. Facultad de Ciencias. Ingeniería Informática, 1997.

[39] M. Garreau, J. L. Coatrieux, R. Collorex, and C. Chardenon. A knowledge based approach for 3-d reconstruction and labeling of vascular networks from biplane angiographic projections. *IEEE Transactions on Medical Imaging*, 10:122–131, 1991.

[40] G. Gensini. *Coronary arteriography in heart disease. A Textbook of Cardiovascular Medicine.* W. B. Saunders Company.E. Braunwald ed., Philadelphia, 1980.

[41] J.C. Gurley, S.E. Nissen, D.C. Booth, M.Harrison, P. Grayburn, J.L. Elion, and A.N. DeMaria. Comparison of simultaneously performed digital and film-based angiography in assessment of coronary artery disease. *Circulation*, pages 1141–1160, 1988.

[42] P. Hall, M. Ngan, and P. Andreae. Reconstruction of vascular networks using three dimensional models. *IEEE Transactions on Medical Imaging*, 16(6):919–929, 1997.

[43] A. Yuille P. Hallinan and D. Cohen. Feature extraction from faces using deformable templates. *International Journal on Computer Vision*, (2):99–111, 1992.

[44] R. M. Haralick and L. G. Shapiro. The consistent labeling problem: Part i. *IEEE Transactions on Pattern Analysis and Machine Intelligence*, 1:173–174, 1979.

[45] R. M. Haralick and L. G. Shapiro. The consistent labeling problem: Part ii. *IEEE Transactions on Pattern Analysis and Machine Intelligence*, 2:193–203, 1980.

[46] Simon Haykin, editor. *Adaptive Filter Theory 3rd Edition.* Prentice Hall Information and System Sciences Series, 1996.

[47] J. Honeyman and E. Staab. *Sillabus: A Special Course in Computers for Clinical Practice and Education in Radiology.* RSNA Publications., 1992.

[48] S.C. Horii and W. D. Bidgood. *PACS Mini Refresher Course: Network and ACR- NEMA Protocols.* Radiographics, 1992.

[49] J. Hoschek and D. Lasser. *Fundamentals of computer Aided Geometric Design.* Wellesley, MA: A.K. Peters, Ltd., 1993.

[50] M. Kass, A. Witkin, and D. Terzopolous. Snakes: Active contour models. *International Conference on Computer Vision. London*, pages 259–268, 1987.

[51] A. Kayser and G.L. Reijns. *A Distributed Database for a Picture Archiving and Communications System.* Proc. SPIE Medical Imaging VI: PACS Design and Evaluation: 1654: 566-572., 1992.

[52] T.E. Kennedy and E.W. Bergholz. *Status of the Camtronics Approach to the Digital Catheterisation Laboratory, in Cardiovascular Imaging, Eds. J.H.C. Reiber and E.E. van der Wall.* Dordrecht: Kluwer Academic Publishers, 1996.

[53] Morton J. Kern. *The Cardiac Catheterization Handbook.* Morgan Kaufmann Publishers. Inc, 1992.

[54] A. Klein, F. Lee, and A. A. Amini. Quantitative coronary angiography with deformable spline models. *IEEE Transactions on Medical Imaging*, 16. no. 5:468–482, 1997.

[55] P.M. Kuzmak and R.E. Dayhoff. A bi-directional acr-nema interface between the va's dhcp integrated imaging system and the siemens-loral pacs. *Comput. Appl. Med. Care*, pages 40–44, 1992.

[56] A. Lanitis, C. J. Taylor, and T. F. Cootes. A unified approach to coding and interpreting face images. *International Conference on Computer Vision*, 5:368–373, 1995.

[57] P. Elliot Larry and K. Mun Seong Et Al. Digital imaging network system. evaluation report. Technical report, Departament of Radiology, Georgetown University Medical Center., March 1990.

[58] Baleriaux Danielle Universite libre Brussels et al. An overview of picture archiving and communication system. Technical report, Report N 1021. Project: AIM - 1030., September 1989.

[59] A. López, R. Toledo, J. Serrat, and J. J. Villanueva. Extraction of vessel centerlines from 2d coronary angiographies. *Proc. of the 8th National Conference on Pattern Recognition and Image Analysis. Bilbao. Spain*, vol 1. no. 11:489–496, 1999.

[60] T. Ma and H. D. Tagare. Consistency and stability of active contours with euclidean and non-euclidean arc lengths. *IEEE Transactions on Image Processing*, vol. 8 no. 11:1549–1559, 1999.

[61] K. V. Mardia, J. T. Kent, and J. M. Bibby, editors. *Multivariate Analysis.* Academic Press. Harcourt Brace & Company Publishers, 1995.

[62] R. Martinez, W. Dallas, and K. Komatsu. *Evaluation and Critique of the ACR-NEMA Standard for Picture Archiving and Communications Systems.* Proc. SPIE Medical Imaging IV: PACS System Design and Evaluation, 1234: 686-693, 1990.

[63] E. Meijering. *Image Enhancement in Digital X-Ray Angiography.* PhD thesis, Image Science Institute, University Medical Center Utrecht (Utrecht, the Netherlands), 2000.

[64] S. Menet, P. Saint-Marc, and G. Medioni. B-snakes: Implementation and application to stereo. *DARPA Image Understanding Workshop*, pages 720–726, 1990.

[65] D. Meyer-Ebrecht. Digital image communication. *European Journal of Radiology*, pages 47–55, 1993.

[66] C. Molina, G. Prause, P. Radeva, and M. Sonka. Catheter path reconstruction from biplane angiography using 3d snakes. *Proceedings SPIE. Medical Imaging*, 1998.

[67] D.R. Musser and A. Saini. *STL Tutorial and Reference Guide: C++ Programming with the Standard Template Library.* Addison-Wesley ISBN 0-201-63398-1., 1996.

[68] J. F. Nealon. *Status of the GE Approach to the Digital Catheterisation Laboratory, in Cardiovascular Imaging, Eds. J.H.C. Reiber and E.E. van der Wall.* Dordrecht: Kluwer Academic Publishers, 1996.

[69] T. V. Nguyen and J. Sklansky. Reconstructing the 3-d medial axes of coronary arteries in single-view cineangiograms. *IEEE Transactions on Medical Imaging*, vol. 13 no. 6, 1994.

[70] S.E. Nissen and et al. Cardiac angiography without cine-film: Erecting a'tower of babel' in the cardiac catheterisation laboratory. acc position statement. *Journal of the American College of Cardiology*, pages 28–37, 1994.

[71] J.B. Olsen. Functional and user requirements for imacs. *Computer Methods and Programs in Biomedicine*, pages 131–134, 1991.

[72] X. Pardo, P. Radeva, and J. Villanueva. Self-training statistic snake for image segmentation and tracking. *Tenth Internation Conference on Image Analysis and Processing*, pages 402–411, 1999.

[73] L. Piegl. Key developments in computer-aided design. *CAD*, 21(5):262–273, 1989.

[74] L. Piegl. *Fundamentals Developments of computer Aided Geometric Modeling.* London, Academic Press., 1993.

[75] P.J. Plauger, A. Stepanov, M. Lee, and D. Musser. *The Standard Template Library.* Prentice-Hall. ISBN 0-13-437633-1, 1996.

[76] R. Poli, G. Coppini, M. Demi, and G. Valli. An artificial vision system for coronary angiography. *Proc. Computers in Cardiology*, pages 17–20, 1991.

[77] G. Prause, X. Zhang, S. DeJong, C. R. McKay, and M. Sonka. Semi-automated segmentation and 3d reconstruction of coronary trees: Biplane angiography and intravascular ultrasound data fusion. physiology and function from multidimensional images. *Proceedings SPIE*, 2709, 1996.

[78] R. S. Pressman. *Software Engineering: A Practitioner's Approach. Third Edition.* McGraw-Hill, 1993.

[79] F. W. Prior. *Specifying DICOM Compliance for Modality Interfaces.* Radiographics, 1993.

[80] J. Puentes, C. Roux, M. Garreau, and J. L. Coatrieux. Dynamyc feature extraction of coronary artery motion using dsa image sequences. *IEEE Transactions on Medical Imaging*, vol. 17 no. 6:857–872, 1998.

[81] P. Radeva. *Model-Based Deformable Shapes for Segmentation, Registration and Tracking*. PhD thesis, Universitad Autonoma de Barcelona, Departmento de Informática, 1996.

[82] P. Radeva, J. Serrat, and E. Marti. A snake for model-based segmentation. *International Conference on Computer Vision. MIT. USA*, pages 816–821, 1995.

[83] P. Radeva, A. Sole, A. Lopez, and J. Serrat. Detecting nets of linear structures in satellite images. *Machine Vision and Advanced Image Processing in Remote Sensing. Springer-Verlag*, pages 304–316, 1999.

[84] P. Radeva, R. Toledo, C. Von Land, and J. Villanueva. 3d vessel reconstruction from biplane angiograms using snakes. *Proc. Computers in Cardiology*, pages 773–776, 1998.

[85] H. Rahms, M. Sanz, M.T. Arredondo, and F. del Pozo. Usability analysis of a telemedicine system for interventional cardiology. *Proc. Computers in Cardiology*, pages 661–664, 1995.

[86] O. Ratib. Papyrus: Image file format specifications, version 2.3. Technical report, Digital Imaging Unit, Center of Medical Informatics, University Hospital of Geneva, 1990.

[87] J. Reiber and P. Serruys, editors. *Progress In Quantitative Coronary Arteriography*. Kluwer Academic Publishers, 1994.

[88] J.H.C. Reiber, G. Koning, P.M.J. van der Zwet, and L. Schiemanck. Inaccuracy of quantitative coronary arteriography when analyzed from s-vhs videotape. *Catheterization and Cardiovascular Diagnosis*, pages 32–38, 1996.

[89] G. L. Reijns and A. Kayser. Communications for a picture archiving communications system with a parallel operating image data base. *Journal of Digital Imaging*, pages 55–64, 1993.

[90] T.A. De Rouen, J.A. Murray, and T. Takaro. Variability in the analysis of coronary arteriograms. *Circulation*, pages 324–328, 1977.

[91] N. Rougon and F. Preteux. Deformable markers: Mathematical morphology for active control models control. *SPIE Image Algebra and Morphological Image Processing*, vol. 1568, 1991.

[92] S. Ruan, A. Bruno, J. L. Coatrieux, and R. Collorex. Estimation de mouvement 3d en coronarogrpahie. *Innovation and Technology in Biology and Medicine*, vol. 14 no. 2:188–198, 1993.

[93] A. Sarwal, A. Dhawan, and Y. Chitre. 3-d reconstruction of coronary arteries using estimation techniques. *Proc. SPIE*, vol. 2434:361–369, 1995.

[94] R. Simon, R. Brennecke, O. Hess, B. Meicr, H. Reiber, and C. Zeelenberg. Report of the esc task force on digital imaging in cardiology. recommendations for digital imaging in angiocardiography. *European Heart Journal*, pages 1332–1334, 1994.

[95] C. Smets, F. van de Werf, P. Sueten, and A. Oosterlinck. An expert system for the labeling and 3d reconstruction of the coronary arteries from two projections. *International Journal of Cardiac Imaging*, 5:145–154, 1990.

[96] I. Sommerville. *Software Engineering, second edition.* Reading, MA: Addison-Wesley Publishing Company, Inc., 1985.

[97] M Sonka, Vaclav Hlavac, and Roger Boyle, editors. *Image Processing, Analysis and Machine Vision.* Chapman & Hall Computing, 1994.

[98] M. Sonka, G. Reddy, and S.M. Collins. Adaptive approach to accurate analysis of small diameter vessels in cineangiograms. *IEEE Transactions on Medical Images*, 16:87–95, 1997.

[99] A. Stepanov and M. Lee. The standard template library. technical report hpl-94-34. Technical report, Hewlett-Packard Laboratories, April 1994.

[100] P. Sueten, C. Smets, G. Verbeek, and A. Oosterlinck. Knowledge based blood vessel delineation on dsa images. *Proceedings SPIE. Medical Imaging II*, 914:406–414, 1988.

[101] Y. Sun. Automated identification of vessel contours in coronary arteriograms by an adaptive tracking algorithm. *IEEE Transactions on Medical Images*, 8:78–88, 1989.

[102] K. Sung and Tomaso Poggio. Example-based learning for view-based human face detection. *A.I. Memo 1521, C.B.C.L. Paper 112*, 1994.

[103] W.H. Tait. *Radiation Detection.* Butterworth & Co (Publishers) Ltd., London UK, 1980.

[104] R. Toledo. Estación de trabajo multimedia para entornos radiológicos. Master's thesis, Universitad Autonoma de Barcelona, Departmento de Informática, 1996.

[105] R. Toledo, X. Orriol, P. Radeva, X. Binefa, J. Vitria, and J. J. Villanueva. Tracking elongated structures using statistical snakes. *Proc. IEEE Computer Vision and Pattern Recognition*, pages 108–120, 2000.

[106] R. Toledo, P. Radeva, C. Von Land, and J. Villanueva. 3d dynamic model of the coronary tree. *Proc. Computers in Cardiology*, pages 777–780, 1998.

[107] R. Toledo, P. Radeva, X. Orriol, X. Binefa, J. Vitria, and J. J. Villanueva. Eigensnakes for vessel segmentation in angiography. *Proc. IEEE International Congress on Pattern Recognition*, pages 108–120, 2000.

[108] R. Toledo and C. D. von Land. Care: Computer assisted radiology environment. *Tecnología de imágenes médicas, Convención iberoamericana sobre la salud en la sociedad global de la información*, pages 108–120, 1996.

[109] M. Turk and A. Pentland. Eigenfaces for recognition. *Journal of Cognitive Neuroscience*, vol. 3(1):71–86, 1991.

[110] J. K. Udupa, H. Hung, D. Odhner, and R. Goncalves. Multidimensional data format specification: A generalization of the american college of radiology - national electric manufacturers association standards. *Journal of Digital Imaging*, pages 26–45, 1992.

[111] K. Vreeswijk. *Philips CD-Medical: A New Era in Digital Cardiac Review, Exchange and Archiving. in Cardiovascular Imaging, Eds. J.H.C. Reiber and E.E. van der Wall.* Dordrecht: Kluwer Academic Publishers, 1996.

[112] A. Wahle, H. Oswald, and E. Fleck. 3d heart-vessel reconstruction from biplane angiograms. *IEEE Computer Graphics and Applications*, pages 65–73, 1996.

[113] A. Wahle, H. Oswald, G. A. Schulze, J. Beier, and E. Fleck. 3d reconstruction, modelling and viewing of coronary vessels. *Computer Assisted Radiology*, pages 669–676, 1991.

[114] J. Weickert. Coherence-enhancing diffusion of colour images. *Image and Vision Computing*, 17:201–212, 1999.

[115] Y. Yanagihara, T. Hashimoto, T. Sugahara, and N. Sugimoto. A new method for automatic identification of coronary arteries in standard biplane angiograms. *International Journal of Cardiac Imaging*, vol. 10:253–261, 1994.

[116] Y.Tronchot. Format des images et connexions des sources. *Annales de Radiologie*, pages 365–374, 1993.

[117] X. Zhang, S. M. Collins, and M. Sonka. Tree pruning strategy in automated detection of coronary trees in cineangiograms. l_1. *Proceedings of International Conference on Image Processing ICIP'95 IEEE*, 17:656–659, 1995.

Publications

- R. Toledo, P. Radeva, X. Orriols, X. Binefa, J. Vitria, J. Villanueva. Eigensnakes for vessel segmentation in angiography. *Proceedings IEEE International Congress on Pattern Recognition, September 2000.*

- J. Mauri, E-F. Nofrerías, B. García del Blanco, E. Iráculis, J.A. Gómez Hospital, J. Comín, M. A. Sanchez Corral, F. Jara, A. Cequier, E. Esplugas, D. Gil, J. Saludes, P. Radeva, R. Toledo, J. Villanueva. Moviment del vas en l'analisi d'imatges de ecografia intracoronária: un model matemátic.*Congrés de la Societat Catalana de Cardiologia, Barcelona, 2000.*

- J. Mauri, E-F Nofrerías, J. Comín, B. García del Blanco, E. Iráculis, J.A. Gómez Hospital, P. Valdovinos, F. Jara, A. Cequier, E. Esplugas, O. Pujol, C. Cañero, D. Gil, P. Radeva, R. Toledo, J. Villanueva. Avaluació del Conjunt Stent/Artéria mitjanant ecografia intracoronária: l'entorn informátic. *Congrés de la Societat Catalana de Cardiologia, Barcelona, 2000.*

- X. Orriols, R. Toledo, X. Binefa, P. Radeva, J. Vitri, J.J. Villanueva. Probabilistic Saliency Approach for Elongated Structure Detection using Deformable Models. *Proceedings IEEE International Congress on Pattern Recognition, September 2000.*

- C. Cañero, P. Radeva, R. Toledo, J.J. Villanueva. 3D Curve Reconstruction by Biplane Snakes. *Proceedings IEEE International Congress on Pattern Recognition, September 2000.*

- R. Toledo, P. Radeva, X. Orriols, X. Binefa, J. Vitria, J. Villanueva. Tracking Elongated Structures Using Statistical Snakes. *Proceedings IEEE International Congress on Computer Vision and Pattern Recognition, June 2000.*

- A. Lopez, R. Toledo, J. Serrat, J. Villanueva. Extraction Of Vessel Centerlines From 2D Coronary Angiographies. 8th National Conference On Pattern Recognition And Image Analysis. *Proceedings AERFAI, May 1999.*

- C. Cañero, P. Radeva, O. Pujol, R. Toledo, D. Gil, J. Saludes, J. Villanueva, B. García del Blanco, J. Mauri, E. F-Nofrerías, J. A. Gómez Hospital , E. Iráculis, J. Comín, C. Quiles, F. Jara, A. Cequier, E. Esplugas. Optimal stent implantation: Three -dimensional Evaluation of the mutual position of stent and vessel via intracoronary ecography. International Conference on Computer in

Cardiology *Proceedings of International Conference on Computer in Cardiology, August 1999.*

- J. Comín, J. Mauri, B. Garcia del Blanco, E. F-Nofrerías, J.A. Gómez, E. Iráculis, C. Quiles, F. Jara, A. Cequier, E. Esplugas, C. Cañero, P. Radeva, R. Toledo, J. Villanueva. Selecció de l'Stent en base a la longitud real de la lesió: un nou métode. *Catalonian Conference on Cardiology, Sagaró, Girona, 1999.*

- E. Iráculis, J. Mauri, B. García del Blanco, E. F. Nofrerías, J.A. Gómez Hospital, J. Comín, C Quiles, F Jara, A Cequier, E Esplugas. O Pujol, P. Radeva, R. Toledo, J. Villanueva. Reconstrucció tridimensional i quantificació de l'arbre coronari utilitzant ecografia intracoronária. *Catalonian Conference on Cardiology, Sagaró, Girona, 1999.*

- B. García del Blanco, J. Mauri, E. F-Nofrerías, J. A. Gómez-Hospital, E. Iráculis, J. Comín, C Quiles, F. Jara, A. Cequier, E. Esplugas, O. Pujol, C. Cañero, P. Radeva, R. Toledo, J. Villanueva. Implantació óptima d'stents: Avaluació tridimensional del conjunt stent/artéria mitjanant ecografia intracoronária. *Catalonian Conference on Cardiology, Sagaró, Girona, 1999.*

- O. Pujol, C. Cañero, P. Radeva, R. Toledo, D. Gil, J. Saludes, J. Villanueva, B. García del Blanco, J. Mauri, E. F-Nofrerías, J. A. Gómez Hospital , E. Iráculis, J. Comín, C. Quiles, F. Jara, A. Cequier, E. Esplugas. Three dimensional reconstruction and quantification of the coronary tree using intravascular ultrasound images. International Conference on Computer in Cardiology. *Proceedings of International Conference on Computer in Cardiology, August 1999.*

- R. Toledo, P. Radeva, C. Von Land, J. Villanueva. 3D Dynamic Model Of The Coronary Tree. International Conference on Computer in Cardiology *Proceedings of International Conference on Computer in Cardiology, September 1998.*

- R. Toledo, C. Von Land, J. Villanueva. TeleRegions: Application of Telematics in Cardiac Care. International Conference on Computer in Cardiology *Proceedings of International Conference on Computer in Cardiology, September 1997.*

- R. Toledo, C. Von Land, J. Villanueva. CARE: Computer Assisted Radiology Environment, Tecnología de Imágenes Médicas. Convención Iberoamericana sobre la Salud en la Sociedad Global de la Información *Proc. Convención Iberoamericana sobre la Salud en la Sociedad Global de la Información, September 1996.*

- R. Toledo, C. Von Land, J. Villanueva TeleRegion: Tele-Applications for European Regions. Experiencias de validación, uso y expansión de la telemática a nivel regional e inter-regional. Convención Iberoamericana sobre la Salud en la Sociedad Global de la Información. *Proc. Convención Iberoamericana sobre la Salud en la Sociedad Global de la Información, September 1996.*

- O. Barbero, Xavier Catasus, Josep Fernandez, Rosa Ruiz, Rafael Valls, R. Toledo, Josep Paradells. Development And Implantation Of Two Teleradiology And Teleconsulting Applications In Catalunya: RAIM and CARE. The fourth international Conference on image management and communication. *Proc. international Conference on image management and communication, August 1995.*

- C. Von Land, R. Toledo, J. Villanueva Object Oriented Design of the DICOM (Digital Imaging and Communications in Medicine) standard. International Symposium on Cardiovascular Imaging. *Proceedings of International Symposium on Cardiovascular Imaging, April 1995.*

- R. Toledo, J.J. Villanueva. Estación de trabajo de radiología. 6th National Conference On Pattern Recognition And Image Analysis. *Proceedings AERFAI, April 1995.*

- J. Agustí Cullell, C. Sierra, J. Pluss, R. Toledo. Operadores de Construcción de Estratégias en Sistemas Expertos. Congreso de la Asociación Española de Inteligencia Artificial. *Proc. AEPIA, October 1989.*